Patterns of sound radiation behind pointlike charged obstacles in plasma flows

P. Guio
Department of Physics and Astronomy, University College London, Gower Street, London WC1E 6BT, United Kingdom

W. J. Miloch
Institute of Theoretical Astrophysics, University of Oslo, Box 1029 Blindern, N-0315 Oslo, Norway
and School of Physics, The University of Sydney, Sydney, NSW 2006, Australia

H. L. Pécseli
Department of Physics, University of Oslo, Box 1048 Blindern, N-0316 Oslo, Norway

J. Trulsen
Institute of Theoretical Astrophysics, University of Oslo, Box 1029 Blindern, N-0315 Oslo, Norway
(Received 5 March 2008; revised manuscript received 14 May 2008; published 3 July 2008; corrected 28 July 2008)

The electrostatic potential and plasma density variations around a pointlike charged object in a plasma flow are studied. These objects can represent small charged dust particles, for instance. The radiation patterns can be interpreted as the result of sound waves being radiated by the obstacle. Two limits are considered: one where the electron-ion temperature ratio is large, $T_e \gg T_i$, and one where $T_e/T_i \approx 1$. The former limit can be described by a simple model based on geometrical optics, while the latter requires a kinetic model in order to account for the effects of ion Landau damping. The results are illustrated by numerical simulation using a particle-in-cell code, where the electrons are treated as an isothermal massless fluid, giving a nonlinear Poisson equation. The analytical results are in good agreement with the numerical simulations.

DOI: 10.1103/PhysRevE.78.016401 PACS number(s): 52.20.−j, 52.65.Rr, 52.27.−h

I. INTRODUCTION

The electrostatic potential surrounding solid objects, such as dust particles, immersed in plasmas depends critically on the plasma conditions [1]. In thermal equilibrium where the objects are at rest, we find the standard electrostatic Debye shielding. When the particles are exposed to streaming plasma, for instance, the conditions can change significantly and noticeable long-range potential variations develop in the wake of the particle. These features are important for the understanding of interactions of two or more objects in the linear as well as nonlinear limits [2,3], and the problem has received great attention [4–7].

In the present study, we consider small, pointlike objects with a fixed charge being exposed to a streaming plasma, or equivalently moving with respect to a plasma. There is no *a priori* requirements of the plasma being in thermal equilibrium, but this is probably the most relevant case. We focus on this scenario by assuming that the electron and ion components can be assigned a temperature, although this need not be the same for the two species. Two limiting cases are considered. First when the electron-ion temperature ratio is large, $T_e \gg T_i$, we can use a fluid model. In this limit, we can use a geometrical optics approach, which gives detailed insight into the physical processes forming the spatial variation in the potential. The other limit, where $T_e \approx T_i$, requires a kinetic treatment in order to include the effects of ion Landau damping. We analyze this case making use of the quasineutral assumption, thereby ignoring potential variations on the electron Debye-length scale. Since the ion Landau damping is strong when $T_e \approx T_i$, these small-scale variations are strongly damped anyhow. The study is supported by results from a numerical particle-in-cell (PIC) simulation, where we assume the electrons to be Boltzmann-distributed at all times as a massless fluid. The expense for this simplification is a nonlinear Poisson equation.

II. FLUID MODEL

A number of studies [4,5] have discussed the variation of the electrostatic potential ϕ behind a moving pointlike object by using a dielectric function. This function is obtained by a linearized analysis of a fluid model with cold ions, $T_i \approx 0$, and warm isothermal electrons at temperature T_e. The wave-number–frequency dependent plasma dielectric function is given here by

$$\varepsilon(\omega,k) = 1 + \frac{1}{(k\lambda_D)^2} - \left(\frac{\Omega_{pi}}{\omega}\right)^2, \tag{1}$$

where Ω_{pi} is the ion plasma frequency and λ_D is the electron Debye length. It is essential that the quasineutral assumption was not used in obtaining Eq. (1).

The form (1) can be used in the Fourier-transformed version of Poisson's equation with an externally imposed moving point charge, and the steady-state spatial variation of ϕ is obtained in the rest frame of the particle. Formally this procedure is correct and gives the desired result, within the implied assumptions, but gives little physical insight. The stationary potential variation in the comoving frame is due to waves being radiated by the source. The wave properties are best explained by a different procedure. Inverting Poisson's equation with Eq. (1) is not a trivial problem, and computational errors can easily occur.

In the present discussion, we will provide qualitative arguments for the appearance of the wave form of dispersive

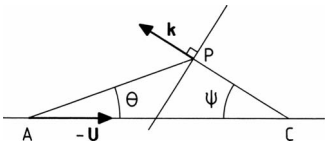

FIG. 1. Illustration of the angles and reference points entering the discussion of radiation of electron plasma waves by a charge moving with constant velocity. The local phase front is shown perpendicular to **k**.

ion sound waves being radiated by a charge moving with constant velocity. Solving $\varepsilon(\omega,k)=0$ to give the natural wave modes, $\omega=\omega(k)$, we find the simple version of the dispersion relation for electrostatic ion sound waves,

$$\omega = \frac{k}{\sqrt{1+k^2}}, \tag{2}$$

written here in dimensionless units with velocities normalized by the sound speed $C_s \equiv \sqrt{\kappa T_e/M}$, frequencies by Ω_{pi}, and wave numbers by $1/\lambda_D$.

The following analysis will be kept in general terms, allowing the arguments to be generalized also to other related problems. We make the following simplifying assumptions: (i) Only one relevant wave type is present, as described by the dispersion relation (2), and (ii) we consider only the "far field" of the wave train, i.e., restrict ourselves to the region more than a wavelength from the source. Finally, by assumption, (iii) we will be concerned only with the qualitative wave form, and not in the precise amplitude distribution. The analysis is based on arguments from geometrical optics. Figure 1 is used for illustrating the analysis. The charged particle is assumed to be at the position A, and the arguments will refer to the comoving coordinate system, in which the wave field will be stationary. The plasma will then be streaming backwards in this frame, as illustrated by the arrow $-\mathbf{U}$ in Fig. 1. We take an arbitrary point P, where the local wave vector $\mathbf{k}$ is drawn, and define the two angles θ and ψ.

Since we assume the wave field to be constant in the comoving frame of reference, we must have $\Omega(\mathbf{k})=\omega(k)-\mathbf{U}\cdot\mathbf{k}=0$ there, with $\omega(k)$ given by Eq. (2), and $\Omega(\mathbf{k})$ is the appropriate dispersion relation in the comoving frame of reference. In particular, the group velocity $\nabla_{\mathbf{k}}\Omega$ is different from $u_g \equiv d\omega/dk$. We have $\nabla_{\mathbf{k}}\Omega(\mathbf{k})=\mathbf{u}_g-\mathbf{U}=u_g\mathbf{k}/k-\mathbf{U}$, making explicit use of the isotropy of the dispersion relation (2). Note our distinction in the notation; $\omega(k)$ is a function of the *magnitude* of k only, while $\Omega(\mathbf{k})$ depends also on the *direction* of $\mathbf{k}$. Referring to Fig. 1, we have the horizontal component of $\nabla_{\mathbf{k}}\Omega$ (along the line AC) to be $u_g\cos\psi-U$, while the vertical (or perpendicular) component is $u_g\sin\psi$.

Since the wave field at the position P is induced by the source in position A, the group velocity vector $\nabla_{\mathbf{k}}\Omega(\mathbf{k})$ must be parallel to the direction of the line AP in Fig. 1. This implies

$$\tan\theta = \frac{u_g\sin\psi}{U-u_g\cos\psi}.$$

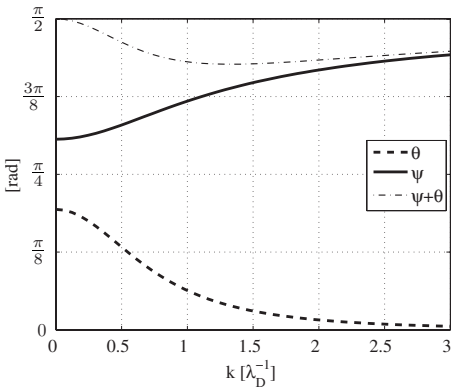

FIG. 2. The variation of the angles θ and ψ with k for a supersonic case with $U=1.75$. The sum $\theta+\psi$ is shown by a thin dashed line.

We have not yet introduced the actual form of the dispersion relation, only its isotropy. We can determine the range of variability of ψ and k from the relation $\Omega(k,\psi)=\omega(k)-Uk\cos\psi=0$. We find

$$\cos\psi = \frac{1}{U\sqrt{1+k^2}}.$$

For $U<1$, we find a limiting minimum wave number,

$$k_0 \equiv \frac{\sqrt{1-U^2}}{U}.$$

The physical meaning of k_0 is readily understood as the crossing point of the dispersion relation (2) and the line $\omega=Uk$. No such limiting wave number exists for $U>1$, at least in the present simplified model.

With $u_g=1/(1+k^2)^{3/2}$, we find after some algebra the relation

$$\tan\theta = \frac{\sqrt{U^2(1+k^2)-1}}{U^2(1+k^2)^2-1}.$$

In Figs. 2 and 3, we show the variation of the two angles θ and ψ with wave number k, for fixed values of U, showing a supersonic as well as the subsonic case.

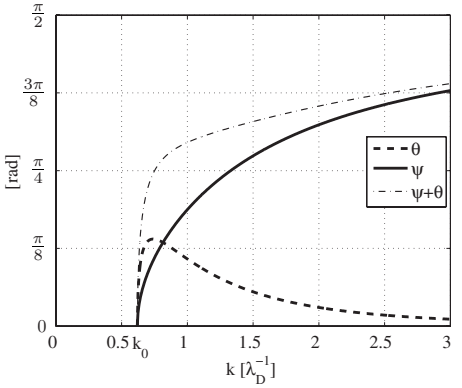

FIG. 3. The variation of the angles θ and ψ with k for a subsonic case with $U=0.85$.

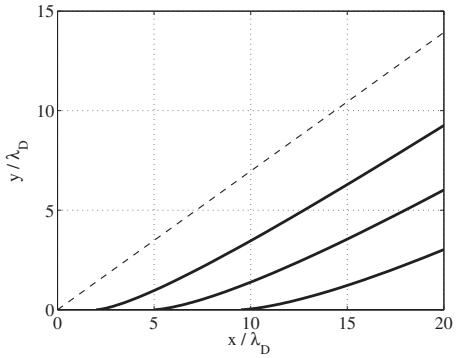

FIG. 4. Illustration for a numerically obtained phase front for the supersonic case, with $U=1.75$. The Mach cone is given by a dashed line. This is also the radiation pattern for the long-wavelength component, at $k\to 0$, as mentioned in the discussion of Fig. 2. The x axis is along the flow direction.

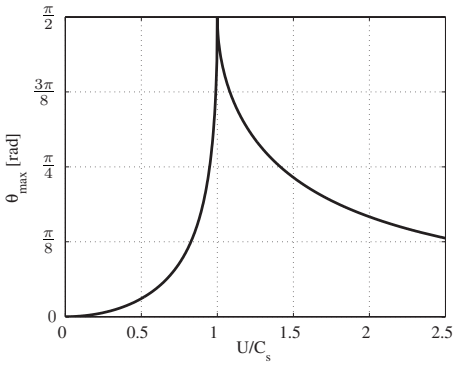

FIG. 5. The variation of the maximum angle $\theta_{\max}$ for varying U.

To apply these results, we first select a direction θ. For given drift velocity U, this choice determines a k value, which subsequently determines ψ, i.e., the direction of the local wave vector **k**. The results differ significantly for sub- and supersonic motions. The full form of the phase fronts can be obtained explicitly. The important point is that these are not needed for a general understanding of the wake properties.

A. Supersonic case

For the supersonic case, we easily find the maximum value of θ to be given by $\sin\theta_{\max}=1/U$, i.e., the Mach condition. Selecting a direction by specifying θ, we find from Fig. 2 that k is uniquely defined, and the radiation pattern behind the obstacle is due to one waveform only.

For the supersonic case, we find the usual Mach cone for very small wave numbers k. In this limit, the line AP is perpendicular to PC, and consequently the phase fronts are parallel to AP. As we let $\theta\to 0$, we find $\psi\to\pi/2$, and here the phase fronts become parallel to the symmetry line AC. There are no oscillations along the line AC for this case. When the angle θ is increased slightly from zero, the radiated wave fronts will exhibit a "cusp" behind the obstacle located at A, as shown in the following.

We can determine the phase fronts being normal to the wave vector **k** in Fig. 1 by $dr/k_\theta=-rd\theta/k_r$ written in cylindrical coordinates for the two-dimensional problem addressed here. The angle between the line AP and the wave vector **k** in Fig. 1 is $\theta+\psi$. We find

$$\frac{dr}{d\theta}=r\tan(\theta+\psi), \tag{3}$$

where ψ is a known function of θ for given Mach number. The result $r=r(\theta)$ is rewritten as $r=r(x,y)$ and shown in Fig. 4. (Note here that the curves represent equiphase contours, not necessarily wave maxima or minima.) These and similar results are obtained by numerical solution of Eq. (3). We note here that the problem is not well posed for $\theta=0$, i.e., at any position along the symmetry axis AC in Fig. 1. Following the dashed and full lines in Figs. 2 and 3, we have that $\theta\to 0$ implies $\psi\to\pi/2$ for $k\to\infty$ giving $dr/d\theta=\infty$ for any r. Alternatively we can have $\psi\to 0$ for $k\to k_0$ giving $dr/d\theta=0$ for any r.

B. Subsonic case

For the subsonic condition, the expression for the radiation cone is more complicated: it corresponds to the k value in Fig. 3, where the angle $\theta=\theta(k)$ has its local maximum. After some algebra, we find the result for $\theta_{\max}$ shown in Fig. 5. The value of k that gives $\theta_{\max}$ is

$$k_m=\frac{\sqrt{2-3U^2+2\sqrt{1-3U^2/4}}}{U\sqrt{3}}.$$

The Mach cone degenerates to a plane when $U=1$. The angle $\theta_{\max}$ is not defined for $U=0$.

At first glance, it might seem confusing that very small velocities U result in a very narrow cone of radiation. We note, however, that in this limit k_0 is very large and the corresponding group velocity vector is almost parallel to the line AC in Fig. 1. Consequently, a signal originating from P can only reach positions in a narrow cone around the line AC. In particular, we note that selecting a direction by giving $0<\theta<\theta_{\max}$, we find from Fig. 3 that for subsonic conditions, actually *two* k values can give the selected θ value. This gives rise to an interference pattern within the radiation cone for $U<1$. The exception is $\theta=0$, where we have one finite solution only, namely k_0.

For the subsonic case, we find that in the limit $k\to k_0$ we have $\theta\approx\psi$, and the two lines AP and CP in Fig. 1 become antiparallel. Along the symmetry line, we find an oscillatory variation with constant wavelength $2\pi/k_0$. For one of the two k solutions, the local phase fronts are perpendicular to the line AC. For the other solution, they form a cusp along AC. At the boundary of the radiated cone, the phase fronts are at an angle to the line AP taken at angle $\theta=\theta_{\max}$: the appearance of the waves in the wake will be reminiscent of the waves trailing a moving ship.

We can also determine the phase fronts by numerical solutions, here with $U<1$. Results are shown in Fig. 6. Note that we find *two* solutions, in agreement with the analytical results previously described, one for each mode. The full

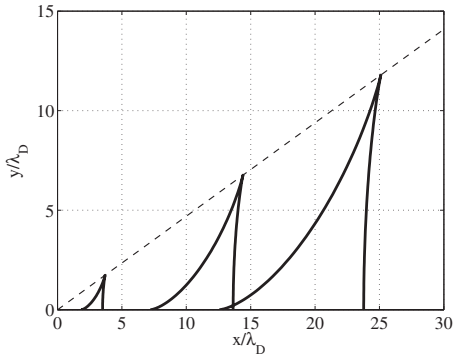

FIG. 6. Illustration for a numerically obtained phase front for the subsonic case, with $U=0.85$. The cone for maximum angle from Fig. 5 is given by a thin dashed line. The x axis is along the flow direction. We have two solutions for the phase fronts as already mentioned in discussing Fig. 3. We show here three sets of equiphase contours; these need not correspond to wave maxima or minima. The positions of the vertical phase fronts of the radiation pattern are periodic along the horizontal axis, with period $2\pi/k_0$, which is 10.14 here, in normalized units.

presentation has a periodicity along the x axis, of length $2\pi/k_0$, with k_0 as given in Sec. II. At $\theta=\theta_{\max}$, the two wave fronts merge since there is only one solution for k at this angle.

The results summarized here are basically consistent with numerical particle-in-cell simulations [8] with Mach numbers 0.8 and 1.6, respectively.

C. Discussions

It is evident that the arguments in Secs. II A and II B are independent of the dimensionality of the problem. Similar arguments may be applied to a point charge and an electric dipole moving in three-dimensional space or on a plane. However, it must be borne in mind that we have only obtained the variation of the surfaces of constant phase. The actual value of the amplitudes along these surfaces will indeed depend on the problem being formulated in two or three spatial dimensions, and also distinguish point charges from electric dipoles. Investigations of a two-dimensional case are sufficient for qualitative results, according to these observations.

The analysis based on Eq. (2) assumes $T_e \gg T_i$. A small but finite value of T_i will modify the results somewhat in the limit of large k, but these corrections will be relatively uninteresting since they are strongly damped. In particular, we find that due to the ion shielding, no radiation pattern develops if $|U|<\sqrt{\kappa T_i/M}$.

Being based on a linear dispersion relation (2), our results here are valid only for small amplitude responses. For the analysis of small-sized objects (smaller than or comparable to the Debye length), these results are appropriate. For large objects, nonlinear effects become important. The ion focusing often observed in numerical studies and experiments on supersonic plasma flows [9] is not present in a linearized model, and it is therefore associated with the nonlinear regime [10,11].

The cusps observed in Figs. 4 and 6 on the line AC correspond to the limit $k\to\infty$. The dispersion relation (2) is very sensitive to finite ion temperatures in this limit, and these cusps will not be observed in laboratory experiments nor realistic numerical simulations.

The analysis presented in this section addresses the same problem as a previous work [12], but the methods are entirely different, and much simpler. The present approach is quite general, and applicable also to other problems.

III. NUMERICAL SIMULATIONS

The results from the studies in Sec. II have been tested by a numerical PIC simulation using large temperature ratios, $T_e/T_i=100$. Such large temperature ratios can be relevant for some discharge experiments [13]. The code has been described and verified by previous studies [14,15], and need not be discussed further here. One special feature of the code is that the electrons are treated as an isothermal massless fluid at all times, in agreement with the assumptions in Eq. (2). The important implication of this model is that only the ion time scale needs to be considered. A consequence of these model assumptions is a nonlinear Poisson equation.

In Fig. 7, we show three results for illustration, all using a temperature ratio of $T_e/T_i=100$. For normalizing lengths, we use the ion Debye length λ_{Di}, where we have $\lambda_D=\lambda_{Di}\sqrt{T_e/T_i}$. The figures show the potential variations behind charged point sources, moving with constant velocity U, considering two subsonic and one supersonic case. The thin dashed lines give the opening angle $\theta_{\max}$ as obtained in Fig. 5. Samples of equiphase contours are also inserted for reference. These numerical results can be seen as full-wave solutions for the problem addressed by geometrical optics in the foregoing analysis.

By inspection of Fig. 7, we find that the basic predictions of the model are well fulfilled. Smaller values of U yield a narrower cone of radiation and a smaller wavelength in the region trailing the point charge. The wave pattern disappears for the supersonic case, and we find the formation of a cusp behind the charged particle as predicted by the study summarized in Sec. II. For $U/C_s=0.42$, we find $\lambda\approx 2.6\lambda_D$ from Fig. 7(a), to be compared with $\lambda_0=2.9\lambda_D$ from the analytical result. Similarly, for $U/C_s=0.75$ we find $\lambda\approx 6.1\lambda_D$ from Fig. 7(b), to be compared with $\lambda_0=7.1\lambda_D$. We find this agreement to be satisfactory, considering that the simulations assume a finite (although small) ion temperature, in variance with the model equation (2).

The simulations that gave Fig. 7 were carried out for given initial conditions, and results are shown at a late time, $\tau=40/\Omega_{pi}$, in the time evolution. In order to improve the signal-to-noise ratio, we averaged five simulation results carried out with the same macroscopic parameters, but with different initialization of the random number generators distributing the particles. Since the analysis is based on a linear model, we take the color-code in arbitrary units on a linear scale.

IV. KINETIC MODEL WITH $T_e/T_i\approx 1$

The fluid model discussed in Sec. II assumes very large temperature ratios, $T_e/T_i\gg 1$. To retain the details of the

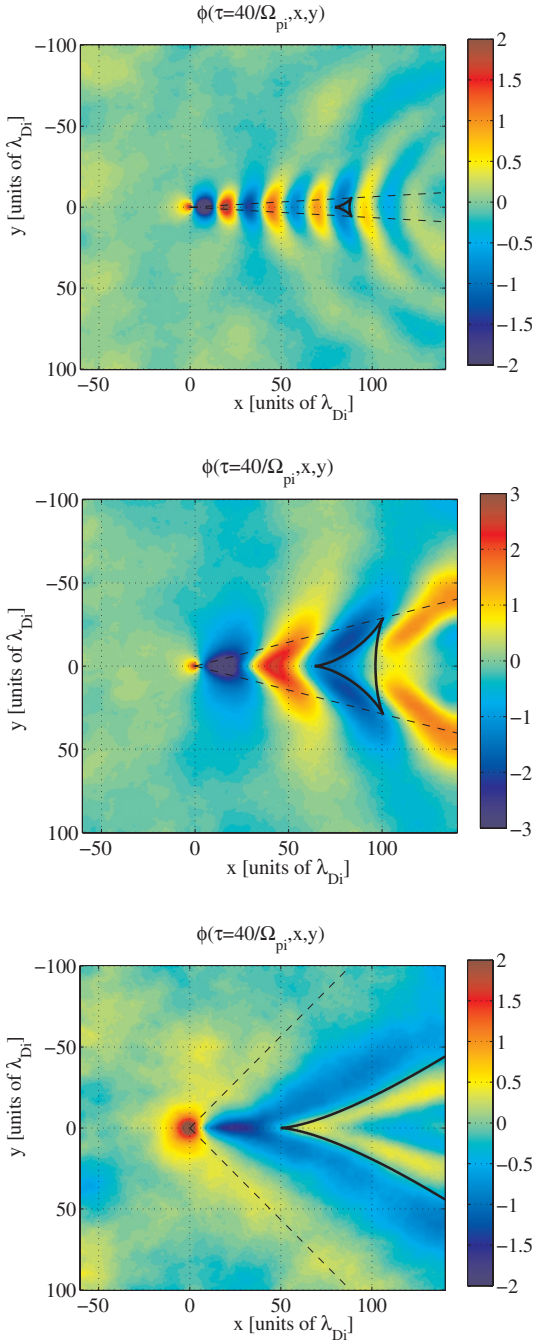

FIG. 7. (Color) Radiation patterns obtained by the PIC code, for the case where $T_e/T_i=100$. We have $U/C_s=0.42$, 0.75, and 1.33. Thin dashed lines give the analytical results for the maximum angles, $\theta_{\max}$ from Fig. 5. Colors are in a linear scale with arbitrary units here and in the following. Lengths are measured in ion Debye lengths, here $\lambda_{Di}=\lambda_D/10$.

wave properties, it is essential to retain Poisson's equation, i.e., we do not impose the quasineutral assumption. In the other limit, $T_e \approx T_i$, the dispersive ripples will disappear due to ion Landau damping, as observed also in laboratory experiments [16]. This limiting case can be analyzed in the quasineutral limit, $n_e \approx n_i \equiv n$, following previous works [14]. In this case, all oscillations in the wake are damped out, and only the Mach cone remains for $U > C_s$, with a form that is distorted due to ion Landau damping. The simple dispersion relation (2) is no longer applicable, and we address the problem by using the linearized ion Vlasov equation, assuming the electrons to be isothermally Boltzmann-distributed at all times, as in the derivation of Eq. (2).

Already here we emphasize one consequence of the assumption of quasineutrality: when Poisson's equation no longer appears in the basic set of equations, we do not have the permittivity of free space, ε_0, entering the list of physical constants. Consequently, we cannot define a Debye length, either for electrons or ions. In the quasineutrality limit, we have no natural quantity of dimension *length* available for normalizing the spatial variables. The only length scale entering originates from the initial or boundary conditions. A δ function does not have any length scale. In the quasineutral limit, we can use arbitrary units for lengths for the problems analyzed in our work.

A. Analysis in one spatial dimension

It is advantageous to consider first the one-dimensional problem, corresponding to a charged slab. We therefore use the one-dimensional version of the ion Vlasov equation, which in its linearized form is

$$\frac{\partial f}{\partial t} + u\frac{\partial f}{\partial x} - \frac{en_0}{M}\frac{\partial \phi}{\partial x}f_0'(u) = 0, \tag{4}$$

where we have introduced the electrostatic assumption by $E=-\partial\phi/\partial x$. We introduced the perturbations in the ion velocity distribution function as $f(x,u,t)$ with the corresponding density perturbation being $n(x,t)=\int_{-\infty}^{\infty} f(x,u,t)du$. To ease the notation, it is here convenient to normalize $\int_{-\infty}^{\infty} f_0(u)du=1$, so that the unperturbed density n_0 appears as a coefficient.

A second relation between f and ϕ can be obtained by using Poisson's equation, containing also the externally imposed charge q, giving

$$\frac{\partial^2 \phi}{\partial x^2} = \frac{e}{\varepsilon_0}\left(n_0\frac{e\phi}{T_e} - \int_{-\infty}^{\infty} f du\right) - \frac{q}{\varepsilon_0}\delta(x)\delta(t), \tag{5}$$

where we introduced the assumption of isothermally distributed electrons. Note that the physical dimension of q is *Coulomb* $\times$ *time*, while for n it is $1/$*length* in the present one-dimensional model. Since the analysis is based on linearized equations, the charge q can be included in a normalizing factor so that ϕ changes sign when q changes sign. Finally, we will assume the fluctuations to be quasineutral, $n_e \approx n_i \equiv n$, and ignore $\partial^2\phi/\partial x^2$ in Eq. (5). The latter approximation assumes all relevant length scales to be larger than the electron Debye length λ_D. We Fourier-transform the resulting equation with respect to position and time, introducing the usual Landau contour. By $\hat{\phi}$, we denote the Fourier-transformed quantity, and find

$$n_0\frac{e\hat{\phi}}{\kappa T_e}=\frac{q/e}{1-\frac{\kappa T_e}{M}\mathrm{P}\int\frac{f_0'(u)}{u-\omega/k}du-i\pi\,\mathrm{sgn}\{k\}\frac{\kappa T_e}{M}f_0'(\omega/k)}, \tag{6}$$

where P$\int$ denotes the principal value of the integral, and sign $\{k\}$ originates from the Landau contour, which is below the singularity for $k>0$ and above it for $k<0$. After some algebra, which is summarized elsewhere [14], we find the space-time varying electrostatic potential by

$$n_0\frac{e\phi(x,t)}{\kappa T_e}=\frac{q/e}{\pi t^2}h'\left(\frac{x}{t}\right), \tag{7}$$

where

$$h(\xi)=\frac{\pi\frac{\kappa T_e}{M}f_0'(\xi)}{\left(1-\frac{\kappa T_e}{M}\mathrm{P}\int\frac{f_0'(u)}{u-\xi}du\right)^2+\left(\pi\frac{\kappa T_e}{M}f_0'(\xi)\right)^2}. \tag{8}$$

When the ion velocity distribution $f(u)$ is a Maxwellian, we can express $h(\xi)$ in terms of the plasma dispersion function Z and its derivative Z' [14,17]. The physical dimension of the variable ξ is *velocity*, i.e., *length*/*time*, while h is dimensionless since the dimension of $f_0'(u)$ is $1/velocity^2$.

The present results are obtained without *a priori* assumptions on the ratio T_i/T_e. By the assumptions of Boltzmann-distributed electrons and quasineutrality, we have $e\phi/\kappa T_e=n/n_0$, except at the position of the moving charge. This implies that our results apply for the relative plasma density perturbations as well.

Now we have the plasma response to a perturbation of the form $q\delta(x)\delta(t)$. This response is denoted $\psi_\delta^{(1)}(x,t)$. The response to a charge moving in one spatial dimension along a path given by $x=Ut$ is found by considering the moving charge as a continuous succession of δ functions. Analytically, this can be written as

$$\begin{aligned}n_0\frac{e\phi(x,t)}{\kappa T_e}&=\int_0^t\int_{-\infty}^{\infty}\delta(x'-Ut')\psi_\delta^{(1)}(x-x',t-t')dx'dt'\\&=\frac{-q/e}{\pi}\int_0^t\frac{1}{(t-t')^2}h'\left(\frac{x-Ut'}{t-t'}\right)dt'\\&=\frac{q/e}{\pi(x-Ut)}h\left(\frac{x}{t}\right),\end{aligned}$$

where by the notation $\psi^{(1)}(x,t)$ we emphasize that we have the response in one spatial dimension. The physical dimension of density is here $1/length$.

The present response is obtained on the basis of a $\delta(x)$-pulse excitation. A dipolar impulse can be preferred [5]. For this case, we can use a $\delta'(x)$ pulse instead, but this is just a trivial modification. The response is linear, and if we differentiate the impulse with respect to x, we obtain the corresponding response by differentiating the result obtained with the original impulse.

B. Results for three spatial dimensions

The one-dimensional response can be interesting in itself, but for realistic physical conditions we require the two-or three-dimensional response. With reference to previous works [4,5], we are primarily interested in the two-dimensional problem, but it turns out to be an advantage to solve for the fully three-dimensional response first.

First we will make the postulate that the response to a perturbation $q\delta(\mathbf{r})\delta(t)$ in three dimensions, as indicated by the superscript (3), has the following form:

$$\psi_\delta^{(3)}(r,t)=\frac{q/e}{t^n}\mathcal{D}^{(3)}\left(\frac{r}{t^m}\right), \tag{9}$$

where $\mathcal{D}^{(3)}$ is a function that is unspecified for the time being.

The response in one dimension can be calculated from the postulated expression (9) as

$$\begin{aligned}&\psi_\delta^{(1)}(x,t)\\&\quad=\frac{q/e}{t^n}\int\int\int_{-\infty}^{\infty}\delta(x')\\&\qquad\times\mathcal{D}^{(3)}\left(\frac{\sqrt{(x-x')^2+(y-y')^2+(z-z')^2}}{t^m}\right)dx'dy'dz'\\&\quad=\frac{\pi q/e}{t^n}\int_{x^2}^{\infty}\mathcal{D}^{(3)}\left(\frac{\sqrt{\gamma}}{t^m}\right)d\gamma,\end{aligned}$$

where first $\xi^2=(y-y')^2+(z-z')^2$ and then $\gamma=\xi^2+x^2$ was introduced. This is now the one-dimensional response to a δ function in time and space. This result *must*, however, be equal to the result obtained in Eq. (7). We therefore have

$$\frac{\pi q/e}{t^n}\int_{x^2}^{\infty}\mathcal{D}^{(3)}\left(\frac{\sqrt{\gamma}}{t^m}\right)\mathrm{d}\gamma=\frac{q}{\pi t^2}h'\left(\frac{x}{t}\right).$$

Differentiating this expression with respect to x, we obtain

$$\frac{1}{t^n}\mathcal{D}^{(3)}\left(\frac{x}{t^m}\right)=-\frac{1}{2\pi^2}\frac{1}{t^4}\left[\frac{t}{x}h''\left(\frac{x}{t}\right)\right]. \tag{10}$$

From this we see that we must have $n=4$ and $m=1$. Therefore, we find

$$\psi_\delta^{(3)}(r,t)=-\frac{q/e}{2\pi^2t^4}\left(\frac{t}{r}\right)h''\left(\frac{r}{t}\right). \tag{11}$$

Note here that the physical dimension of h'' is $(time/length)^2$. It is implicit in the arguments that the distribution function $f_0(u)$ is isotropic, i.e., it is the same no matter what direction we use as a reference. Some simple anisotropies are easily incorporated, though. Note the *self-similarity* of this result; it depends on the ratio r/t rather than r and t separately, and it is *scaled* by the factor t^{-4}.

The response to a moving charge in three dimensions can now be calculated in the same way as for the one-dimensional case. The charge is assumed to be moving in the positive z axis with speed U. This yields

$$n_0\frac{e\phi(r,z,t)}{\kappa T_e} = -\frac{q/e}{2\pi^2}\int_0^t \frac{1}{(t-t')^4} \times \frac{t-t'}{\sqrt{r^2+(z-Ut')^2}} h''\left(\frac{\sqrt{r^2+(z-Ut')^2}}{t-t'}\right)dt', \tag{12}$$

where r is the radial coordinate perpendicular to the z axis. This expression can easily be evaluated numerically.

For a point charge which has been moving with constant velocity for a long time, we can simplify Eq. (12) in the rest frame of the particle, taking the origin to be at Ut, to give the result

$$n_0\frac{e\phi(r,z)}{\kappa T_e} = -\frac{q/e}{2\pi^2}\int_0^\infty \frac{1}{\gamma^4}\frac{\gamma}{\sqrt{r^2+(z-U\gamma)^2}} \times h''\left(\frac{\sqrt{r^2+(z-U\gamma)^2}}{\gamma}\right)d\gamma, \tag{13}$$

where we used that $h''(\xi)$ decays for large values of the argument. Due to the assumptions of Boltzmann-distributed electrons and quasineutrality, we have $n_0 e\phi(r,z)/\kappa T_e = n(r,z)$ consistent with the physical dimension of $1/length^3$ of the right-hand side of Eq. (13). Evidently, as expected, the disturbance induced by the moving charge is propagating with velocity U, having a constant spatial shape.

C. Results in two spatial dimensions

Many numerical simulations are restricted to two spatial dimensions [10,18], such as those shown in Sec. III. In order to make a comparison with these results, we derive the radiation pattern also for this case. The procedure is entirely similar to the one used in Sec. IV B. We note here that the two-dimensional response to $q\delta(\mathbf{r})\delta(t)$ can be obtained by a straightforward integration of the three-dimensional response (11) as

$$\begin{aligned}\psi_\delta^{(2)}(r,t) &= \int\int\int_{-\infty}^{\infty} \delta(x')\delta(y') \times \psi_\delta^{(3)}\left(\sqrt{(x-x')^2+(y-y')^2+(z-z')^2},t\right)dx'dy'dz' \\ &= -\frac{q/e}{2\pi^2 t^3}\int_{-\infty}^{\infty}\frac{1}{\sqrt{r^2+\gamma^2}}h''\left(\frac{\sqrt{r^2+\gamma^2}}{t}\right)d\gamma \\ &= -\frac{q/e}{2\pi^2 t^3}\int_{-\infty}^{\infty}\frac{1}{\sqrt{(r/t)^2+\xi^2}}h''\left(\sqrt{(r/t)^2+\xi^2}\right)d\xi \\ &\equiv -\frac{q/e}{2\pi^2 t^3}g\left(\frac{r}{t}\right),\end{aligned} \tag{14}$$

with $r^2 \equiv x^2+y^2$. The functions $h''(\xi)/\xi$ and $g(\xi)$ are shown in Fig. 8 for a Maxwellian $f(u)$. (The physical dimension of the two functions is not the same, so the relative amplitudes cannot be compared.) Apart from the variation close to the origin, we find no significant differences between the two functions, demonstrating that two-dimensional simulations

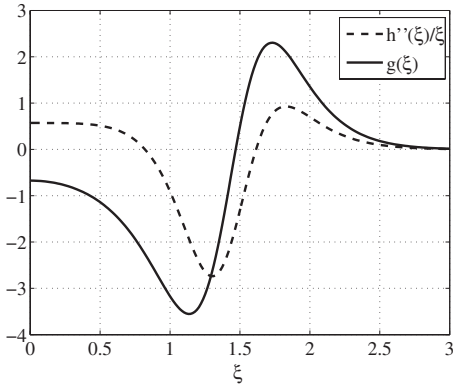

FIG. 8. The two functions $h''(\xi)/\xi$ (dashed line) and $g(\xi)$ (full line) obtained for a Maxwellian $f(u)$, with $T_e/T_i=1$.

of this problem are sufficient to reproduce the most important scales of spatial variation in the problem. The main difference is the time scaling being t^{-4} in three dimensions, while it is with t^{-3} for two spatial dimensions.

As before, we now find the response to a point charge moving along the y axis with a velocity U. In the time-asymptotic limit, we have

$$n_0\frac{e\phi(x,y)}{\kappa T_e} = -\frac{q/e}{2\pi^2}\int_0^\infty \frac{1}{\gamma^3}g\left(\frac{\sqrt{x^2+(y-U\gamma)^2}}{\gamma}\right)d\gamma. \tag{15}$$

In the quasineutral limit, we have no natural length scale for normalizing the x and y variables, as mentioned before. If we introduce an angle ξ so that $x=r\cos\xi$ and $y=r\sin\xi$, we can rescale the length so that $r\to Nr$. We can then scale the integration variable correspondingly, i.e., $\gamma\to N\gamma$. The only consequence of this rescaling will be that the amplitude of $\phi(r,\xi)$ is changed by a factor N^{-2} everywhere, the spatial variation being unchanged otherwise. The spatial damping is consequently not exponential, which could otherwise have been an expected result.

The response to a dipolar perturbation can be relevant also here [5]. We can replace $\delta(r)=\delta(x)\delta(y)$ by $\delta'(x)\delta(y)$, corresponding to an electric dipole aligned with the x axis. Since the analysis is based on a linearized model, we can also readily obtain here the response by differentiating Eq. (15) with respect to x. The three-dimensional result (13) can be generalized similarly.

In Fig. 9, we show a result based on the analytical expression (15) for $T_e/T_i=1$ and $U=1.33C_s$. The central part around $(x,y)=(0,0)$ is saturated to emphasize the asymptotic region where the ion-Landau damping is important. In Fig. 10, we show a result from a numerical PIC particle simulation, here for $T_e/T_i=1$ and $U=1.33C_s$, using the same code as for obtaining Fig. 7. We note the presence of a radiation pattern closely resembling the one found analytically. The ion Landau damping gives a significant modification of the result as compared to the cold ion model summarized in the first part of this work. The analytical results do not apply for distances smaller than a few Debye lengths from the point charge because of the assumption of quasineutrality. This assumption is not made in the numerical simulation, and the results of Fig. 10 consequently have a wider range of appli-

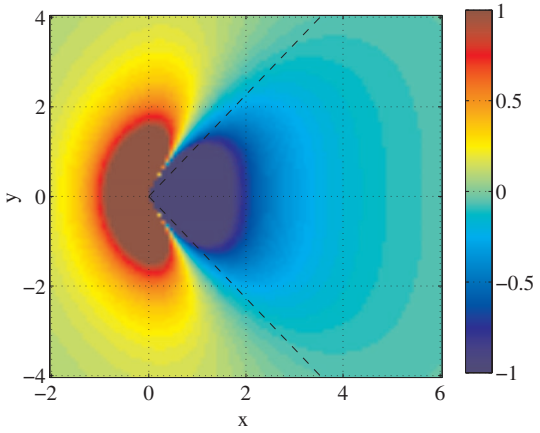

FIG. 9. (Color) Radiation pattern obtained by a linearized kinetic model for $T_e/T_i=1$, by use of the analytical expression (15). Dashed lines give the Mach cone obtained by fluid theory. Coordinates are in arbitrary units, as discussed in the text. We have $U=1.33C_s$.

cability. The slight difference in the position of the maximum potential in Figs. 9 and 10 is a consequence of the quasineutral assumption in Fig. 9. In particular, we have a natural length scale λ_{Di} for normalizing length scales when Poisson's equation is retained in the simulations. If we let $U<C_s$ in these simulations, we find a result resembling the trivial Debye shielding. This result implies that the shielding cloud is only slightly distorted as long as the velocity is between the ion sound speed and the ion thermal speed, $C_s>U>u_{thi}$. For even smaller velocities, the changes are minute as compared to a standard Debye shielding.

V. CONCLUSIONS

We have analyzed the radiation pattern behind point charges moving through unmagnetized plasmas, considering two limiting cases: $T_e/T_i \gg 1$ and also $T_e \approx T_i$. The former case can be analyzed by a simple dielectric model giving Eq. (2), while the latter case requires a kinetic analysis due to the

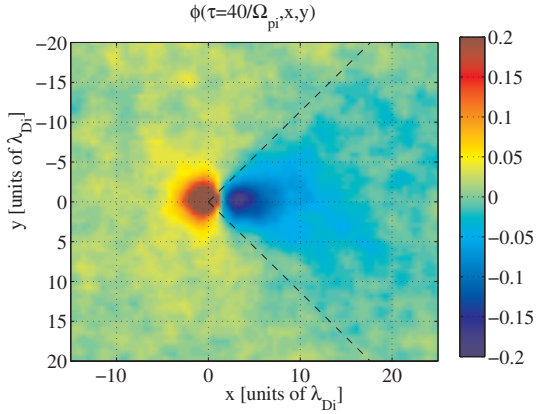

FIG. 10. (Color) Radiation pattern obtained for $T_e/T_i=1$ by a numerical particle simulation with a supersonic velocity, $U=1.33C_s$. The normalizing length scale, λ_{Di}, is the ion Debye length also here.

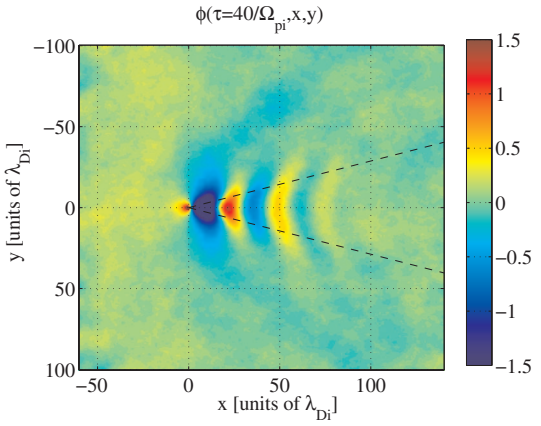

FIG. 11. (Color) Radiation pattern obtained for $T_e/T_i=25$ by a numerical particle simulation with subsonic velocity. We have $U=0.75C_s$.

importance of ion Landau damping. In studying the limit $T_e/T_i \gg 1$ we used a geometrical optics [or the Wentzel-Kramers-Brillouin (WKB)] limit. Formally this assumption limits the applicability of the results to scales much larger than the wavelengths, but by comparison with Fig. 7 we find a good agreement except at the edges of the limiting cones. It seems to be a general experience that the WKB model has a wider range of applicability than expected from its basic assumptions [19].

The potential variation around a charged object moving through plasma media is important for understanding the interaction of two or more charged particles, for the interaction of small charged dust particles in particular [1]. Our results demonstrate that for subsonic charged particles, a noticeable potential variation develops in the wake of such particles, making a long-range interaction possible, provided the temperature ratio T_e/T_i is large. In this case, a trailing particle will experience a potential variation induced by the first one even for separations exceeding several electron Debye lengths; see, for instance, Fig. 7. For small temperature ratios $T_e \approx T_i$, the ion Landau damping reduces the potential variation in the wake of subsonic particles, until it completely disappears for $T_e=T_i$. For this case, we have basically a Debye shielding of a point charge due to finite electron and ion temperatures. A significant potential variation can be found only for supersonic particles, giving the usual Mach cone. Even in this case, we find that the potential variation has a limited spatial range due to the ion Landau damping.

We have varied the electron-ion temperature ratio to determine an approximate transition temperature ratio, where the radiation pattern develops behind a subsonically moving object. For $T_e/T_i=50$, we see no principal differences with the subsonic results in Fig. 7. For $T_e/T_i=10$, on the other hand, we note only one period of oscillation, and we might conclude that the ion Landau damping is effective at this temperature ratio. By trying different parameters, we suggest that a transition temperature of $T_e/T_i=25$ can be used for separating the necessity of choosing kinetic rather than fluid models. As an illustration, we show in Fig. 11 results for $T_e/T_i=25$ and $U=0.75C_s$, where we see the development of oscillations behind the point charge. Also this figure is an

average of five simulations with different initializations of the random number generators. The oscillations are still damped somewhat by ion-Landau damping as compared to Fig. 7, but several wavelengths are clearly discernible. Evidently, the transition temperature ratio discussed here has no unique definition, and depending on the relevant applications, other values can be used.

The results in the present work are restricted by using a linearized response model. For pointlike objects (i.e., diameters much smaller than the electron Debye length) this limitation may be of little consequence. For larger particles, the wake-field is significantly modified due to the large number of electrons and ions absorbed on the surface of the particles [10,11,20] and the linear-response model is no longer applicable. In this limit, we can expect noticeable potential variations to develop in the wake of moving particles, allowing for an interaction potential that is not accounted for by our linear models. The results for conductors and insulators will be significantly different, while this distinction is irrelevant for pointlike objects.

The charged particle loses kinetic energy by exciting the wave pattern. The resulting deceleration is not discussed here. In order to calculate the wave electric field correctly at the particle position, we have to abandon the assumption of quasineutrality. In the present model, we note that $\phi(0,0)$ is singular since the integrals in Eq. (13) as well as in Eq. (15) diverge at this position.

ACKNOWLEDGMENTS

This work was supported in part by the Norwegian Research Council, NFR, while one author (P.G.) was supported by the UK Scientific and Technological Facilities Council (STFC). One of the authors (H.L.P.) thanks Professor K. B. Dysthe for valuable discussions of surface water waves trailing a moving ship.

[1] P. K. Shukla and A. A. Mamun, *Introduction to Dusty Plasmas* (Institute of Physics Publishing, Bristol, 2002).
[2] G. Lapenta, Phys. Scr. **64**, 599 (2001).
[3] G. Lapenta, Phys. Rev. E **66**, 026409 (2002).
[4] O. Ishihara and S. V. Vladimirov, Phys. Plasmas **4**, 69 (1997).
[5] O. Ishihara, S. V. Vladimirov, and N. F. Cramer, Phys. Rev. E **61**, 7246 (2000).
[6] G. Lapenta, Phys. Rev. E **62**, 1175 (2000).
[7] S. V. Vladimirov and M. Nambu, Phys. Rev. E **64**, 026403 (2001).
[8] D. Winske, W. Daughton, D. S. Lemons, and M. S. Murillo, Phys. Plasmas **7**, 2320 (2000).
[9] K. R. Svenes and J. Trøim, Planet. Space Sci. **42**, 81 (1994).
[10] W. J. Miloch, H. L. Pécseli, and J. Trulsen, Nonlinear Processes Geophys. **14**, 587 (2007).
[11] W. J. Miloch, H. L. Pécseli, and J. Trulsen, Phys. Rev. E **77**, 056408 (2008).
[12] J. R. Sanmartin and S. H. Lam, Phys. Fluids **14**, 62 (1971).
[13] K. Takahashi, T. Oishi, K. Shimomai, Y. Hayashi, and S. Nishino, Phys. Rev. E **58**, 7805 (1998).
[14] P. Guio and H. L. Pécseli, Phys. Plasmas **10**, 2667 (2003).
[15] P. Guio, S. Børve, H. L. Pécseli, and J. Trulsen, Ann. Geophys. **18**, 1613 (2001).
[16] P. Michelsen and H. L. Pécseli, Phys. Fluids **16**, 221 (1973).
[17] B. D. Fried and S. D. Conte, *The Plasma Dispersion Function* (Academic, New York, 1961).
[18] F. Melandsø and J. Goree, Phys. Rev. E **52**, 5312 (1995).
[19] R. J. Armstrong, Å. Fredriksen, H. L. Pécseli, and J. Trulsen, Plasma Phys. Controlled Fusion **26**, 703 (1984).
[20] P. Guio and H. L. Pécseli, Ann. Geophys. **23**, 853 (2005).